The published version of the paper "Seymour M.J. Spence, Massimiliano Gioffrè, Ahsan Kareem, An efficient framework for the reliability-based design optimization of large-scale uncertain and stochastic linear systems, Probabilistic Engineering Mechanics, Volume 44, 2016, Pages 174-182, ISSN 0266-8920" is available at: https://doi.org/10.1016/j.probengmech.2015.09.014.

An Efficient Framework for the Reliability-Based Design Optimization of Large-Scale Uncertain and Stochastic Linear Systems

Seymour M.J liano Gioffrè[b], Ahsan Kareem[c]

[a] *Department of Civil and Environmental Engineering, University of Michigan, Ann Arbor, MI 48109, USA*
[b] *CRIACIV/Department of Civil and Environmental Engineering (DICA), University of Perugia, via G. Duranti 93, 06125 Perugia, Italy*
[c] *NatHaz Modeling Laboratory, Department of Civil and Environmental Engineering and Earth Sciences, University of Notre Dame, Notre Dame, IN 46556, USA*

Abstract

This paper is focused on the development of an efficient reliability-based design optimization algorithm for solving problems posed on uncertain linear dynamic system characterized by large design variable vectors and driven by non-stationary stochastic excitation. The interest in such problems lies in the desire to define a new generation of tools that can efficiently solve practical problems, such as the design of high-rise building in seismic zones, characterized by numerous free parameters in a rigorously probabilistic setting. To this end a novel decoupling approach is developed based on defining and solving a limited sequence of deterministic optimization sub-problems. In particular, each sub-problem is formulated from information pertaining to

*Corresponding author
Email addresses: smjs@umich.edu (Seymour M.J. Spence), massimiliano.gioffre@unipg.it (Massimiliano Gioffrè), kareem@nd.edu (Ahsan Kareem)
[1]Tel. +1-734-764-8419, Fax +1-734-764-4292

a single simulation carried out exclusively in the current design point. This characteristic drastically limits the number of simulations necessary to find a solution to the original problem while making the proposed approach practically insensitive to the size of the design variable vector. To demonstrate the efficiency and strong convergence properties of the proposed approach, the structural system of a high-rise building defined by over three hundred free parameters is optimized under non-stationary stochastic earthquake excitation.
Keywords: Reliability-based design optimization, Stochastic loads, Reliability analysis, Monte Carlo simulation, Earthquake engineering, Structural optimization, High dimensional problems

1. Introduction

The benefits that can be achieved in terms of both performance as well as cost reduction through the application of numerical optimization to engineering problems are well known. In order to apply these methods to the design of optimal structural systems subject to environmental loads such as wind and earthquakes, the inherently dynamic and aleatory nature of the system and loads must be rigorously modeled. Indeed, it is well known that there is considerable uncertainty not only in the external environmental excitation but also in the parameters and models describing the system [1]. Recently, considerable effort has been placed on defining reliability-based/robust optimization approaches that describe the performance of the system in a rigorously probabilistic and dynamic setting [1, 2, 3, 4, e.g.], see also [2] for a review. The recent interest in defining these approaches is a direct conse-

quence of the latest computational advances that have opened the door to the possibility of solving problems that only recently would have been considered intractable. A hurdle that has remained a challenge is the possibility of solving reliability-based design optimization (RBDO) problems that are characterized by large design variable vectors. Indeed, of the methods so far developed, very few have considered problems with more than a handful of free design parameters [2]. This can be an important limitation as many practical applications are characterized by large design variable vectors, e.g. the design of typical multistory building systems. The difficulty in efficiently solving reliability-based design optimization, or robust optimization problems, with large design variable vectors is primarily due to how this limits the possibility of efficiently exploring how the probabilistic performance functions vary as the design variable vector changes during the optimization loop. Indeed, if the design variable vector has high dimensions, then surrogate/metamodel-based approaches [2] tend to become intractable as the exploration of the design space necessary to build the surrogate/metamodel will require a prohibitively large number of probabilistic performance evaluations. A similar curse of dimensionality also affects methods based on augmenting the uncertain vector with the design variables, as it becomes increasingly difficult to identify the regions of the design space that contain the optimal solutions. Another approach that has been widely adopted for solving RBDO problems is that based on decoupling the inherently nested probabilistic analysis from the optimization loop [5, 6, 7, 1, 2, 8]. In general, this can only be approximately achieved and requires the sequential application of probabilistic analysis followed by the resolution of an approximate

optimization sub-problem. The crucial point in these approaches is the construction of the sub-problem that generally requires additional information to be gathered on the local behavior of the performance functions around the current design point, e.g. through local random exploration or sensitivities. It is this phase that generally becomes troublesome as the design variable vector increases in size. In this paper a novel decoupling approach is developed that is practically insensitive to the size of the design variable vector. In particular, the methodology is specifically developed for high-dimensional uncertain linear dynamic systems driven by stochastic excitation. As an example of such a system, a case study is considered that focuses on the optimum design of the structural system of a high-rise building subject to non-stationary stochastic earthquake excitation.

2. Formulation of the optimization problem

The optimization problems that are pertinent to this research may be posed in the following form:

$$\text{Find} \qquad \mathbf{x} = \{x_1, ..., x_m\}^T \tag{1}$$

$$\text{to minimize} \qquad W = f(\mathbf{x}) \tag{2}$$

$$\text{s. t.} \quad P_{f_j}(\mathbf{x}) \leq P_{0_j} \quad j = 1, ..., N_c \tag{3}$$

$$x_i \in \mathbf{X}_i \quad i = 1, ..., m \tag{4}$$

where $\mathbf{x}$ is an m-dimensional vector of deterministic parameters defining the design of the system, e.g. the section sizes, W is a deterministic and explicit (in terms of the design variable vector $\mathbf{x}$) cost function associated with the

structural system, P_{f_j} are the failure probabilities associated with the N_c reliability constraints defining the performance of the system, P_{0_j} are the acceptable failure probabilities defining the target reliability of the system, while $\mathbf{X}_i$ is the discrete set to which the ith design variable must belong.

What makes the above outlined RBDO problem difficult to solve are the reliability constraints of Eq. (3). Indeed, the evaluation the aforementioned constraints requires the calculation of the failure probabilities P_{f_j} given by:

$$P_{f_j}(\mathbf{x}) = \int_{\Omega_{F_j}(\mathbf{x})} p(\mathbf{u}) d\mathbf{u} \tag{5}$$

where Ω_{F_j} is the failure domain of the failure event F_j within the space of the uncertain parameters contained in the vector $\mathbf{U}$, while $p(\mathbf{u})$ is the joint probability function of $\mathbf{U}$. In this work the random vector $\mathbf{U}$ describes all uncertainties involved in the system (model and loading parameters). In other words the components of the vector $\mathbf{U}$ represent the uncertain structural parameters and the random variables used in the characterization of the stochastic excitation. Therefore $\mathbf{U}$ will have high dimensions (order of thousands) which excludes the possibility of using analytical approximations, such as first and second order reliability methods, in the calculation of the probabilistic integral of Eq. (5) as they will become computationally intractable [9]. This implies that Eq. (5) must be evaluated using simulation methods and therefore through repeated evaluation of the system response. For practical dynamic systems, this fast becomes computationally cumbersome, especially when it is observed that P_{f_j} is in general an implicit function of $\mathbf{x}$ therefore hindering the calculation of the gradients necessary if efficient gradient-based optimization methods are to be used to solve the optimization problem.

3. Response estimation

3.1. Damage model

The failure events, F_j, of interest to this work may be written in the following form:

$$F_j(\mathbf{x}, \mathbf{u}) = \{d_j(\mathbf{u}, \mathbf{x}) > 1\} \tag{6}$$

where d_j is the damage measure associated with the jth reliability constraint and defined as follows:

$$d_j(\mathbf{u}, \mathbf{x}) = \max_{t \in [0,T]} \frac{|R_j(t; \mathbf{u}, \mathbf{x})|}{C_j} \tag{7}$$

where T is the duration of the event, $R_j(t)$ is the structural response process associated with the jth failure mode while C_j is a measure of the capacity of the system in the jth failure mode. In particular, C_j is directly related to the concept of fragility as defined in [10], i.e. as the conditional probability of having a predetermined damage state, DS_j, given a certain response level r. Indeed, if the capacity C_j is measured in terms of the response thresholds at which the damage state associated with the jth reliability constraint occurs, then the following holds:

$$\text{Fragility}_{DS_j} = P(DS_j | r_j) = P(C_j \leq c_j) \tag{8}$$

where $r_j = c_j$. Therefore the distribution of C_j is simply given by the fragility curve associated with the damage state of interest. The relation of Eq. (8) illustrates how the damage ratio of Eq. (7), and in particular C_j, can be modeled using the extensive fragility databases reported in [11] for a number of common structural and non-structural building components.

By using the damage model of Eq. (7), a predefined damage state will occur if d_j is larger than 1. Therefore the following limit sate function can be assumed for identifying the initiation of damage:

$$g_j(\mathbf{u}, \mathbf{x}) = 1 - d_j(\mathbf{u}, \mathbf{x}) \tag{9}$$

while the failure probabilities are given by:

$$\begin{aligned} P_{f_j}(\mathbf{x}) =& P(g_j(\mathbf{u}, \mathbf{x}) \leq 0) \\ =& \int_{g_j(\mathbf{u},\mathbf{x}) \leqslant 0} p(\mathbf{u}) \mathrm{d}\mathbf{u} \end{aligned} \tag{10}$$

In order to evaluate this integral, the response process $R_j(t)$ needs to be evaluated.

3.2. Load-effect model

In order to model the dynamic response of the system in a generic response parameter R_j (e.g. displacement, interstory drift, stress component), the following linear load-effect model is considered:

$$R_j(t) = s_1 \mathbf{\Gamma}_{R_j}^T \mathbf{K} \mathbf{\Phi}_n \mathbf{q}_n(t) \tag{11}$$

where s_1 is an uncertain parameter modeling the epistemic uncertainties in using a load-effect model of this type, $\mathbf{\Gamma}_{R_j}$ is a vector of influence coefficients indicating the response in R_j due to a unit static force applied one-by-one to the various degrees of freedom of the nominal (mean) system, $\mathbf{K}$ is the nominal (mean) stiffness matrix, $\mathbf{\Phi}_n = [\phi_1, \ldots, \phi_n]$ is the mode shape matrix containing the structure's first n mode vectors while $\mathbf{q}_n = \{q_1(t), \ldots, q_n(t)\}^T$ is the vector containing the first n modal displacement responses given by

solving the following modal equations:

$$\ddot{q}_j(t) + 2s_{3_j}\zeta_j s_{2_j}\omega_j \dot{q}_j(t) + \left(s_{2_j}\omega_j\right)^2 q_j(t) = \frac{\boldsymbol{\phi}_j^T \mathbf{M} \boldsymbol{i} a_g(t)}{m_j} = \frac{Q_j(t)}{m_j} \tag{12}$$

where ω_j, m_j, ζ_j and $Q_j(t)$ are the jth modal circular frequency, modal mass, damping ratio and generalized force respectively, $\mathbf{M}$ is the mass matrix of the system, a_g denotes the time history of the ground motion acceleration, $\boldsymbol{i}$ is the vector of earthquake influence coefficients. The parameters s_{2_j} and s_{3_j} are unit mean uncertain parameters modeling, in the first case, the uncertainty in ω_j due to randomness in the stiffness and mass matrix and in the second case the significant uncertainties that generally affect ζ_j [12, 13].

An efficient way to directly integrate the modal equations is through the concept of digital filters [14, 15]. This method is based on the following transfer function in the complex Laplace domain:

$$H_j(\gamma) = \frac{1}{\gamma^2 + 2s_{3_j}\zeta_j s_{2_j}\omega_j \gamma + \left(s_{2_j}\omega_j\right)^2} \tag{13}$$

where γ is the complex Laplace variable. The characteristic efficiency of digital filters in solving Eqs. (12) is due to the discrete and evenly spaced nature of most experimental/simulated data. The accuracy of the method depends solely on the assumptions made with respect to how the generalized forcing function, $Q_j(t)$, is assumed to vary between two successive data points. Arguably the most convenient assumption is to consider a linear variation (ramp invariant simulation) yielding the following Z-transform function:

$$\tilde{H}_j(z) = \frac{(z-1)^2}{\Delta t\, z} Z \left\{ L^{-1} \left[\frac{1}{\gamma^2 \left(\gamma^2 + 2s_{3_j}\zeta_j s_{2_j}\omega_j \gamma + (s_{2_j}\omega_j)^2\right)} \right] \right\} \tag{14}$$

where Δt is the sampling interval, L^{-1} indicates the inverse of the Laplace transform while z is the generally complex Z-plane variable. Eq. (14) may be written in the form of a second order digital filter:

$$\tilde{H}_j(z) = \frac{b_{0j} + b_{1j}z^{-1} + b_{2j}z^{-2}}{1 + a_{1j}z^{-1} + a_{2j}z^{-2}} \tag{15}$$

where b_{0j}, b_{1j}, b_{2j}, a_{1j} and a_{2j} are jth mode's filter coefficients. From Eq. (15) the following recursive relationship may be defined for the generalized displacement response in the discrete time instant t_i:

$$\begin{aligned} q_j(t_i) = b_{0j}\frac{Q_j(t_i)}{m_j} + b_{1j}\frac{Q_j(t_{i-1})}{m_j} + b_{2j}\frac{Q_j(t_{i-2})}{m_j} \\ - a_{1j}q_j(t_{i-1}) - a_{2j}q_j(t_{i-2}) \end{aligned} \tag{16}$$

The efficiency of this method for digital data with constant sampling frequency is in that the coefficients of Eq. (16) need to be estimated only once. A similar recursive expression may be derived for $\dot{q}_j(t)$ while $\ddot{q}_j(t)$ may be derived from Eq. (12) once $q_j(t)$ and $\dot{q}_j(t)$ are known. It should be observed that the only approximation in the integration scheme outlined above is in the piecewise linear approximation of the generalized forcing function $Q_j(t)$. Therefore, if an adequate sampling frequency is adopted, this method guarantees not only efficiency but also consistency.

3.3. Stochastic ground motion

In order to calculate the response of the system, realizations of the ground motion accelerations $a_g(t)$ are needed. These may be modeled through an appropriate stochastic ground motion model. In this work, a point-source model [16, 17] is adopted, even though it should be observed that the choice

of the ground motion model does not affect the optimization method developed in this work. In particular, the model considered here is described by a radiation spectrum, $A(f; M, r)$, and an envelope function, $e_t(t; M, r)$, which both depend on the moment magnitude, M, and the shortest distance, r, to the fault plane. In order to generate a realization of $a_g(t)$ following this model, a white noise sequence $\mathbf{Z} = [Z_w(i\Delta t) : i = 1, 2, ..., N_T]$ is first generated and modulated by $e_t(t; M, r)$ before being transformed into the frequency domain. Once in the frequency domain, it is first normalized by the square root of the mean square of $A(f; M, r)$ and then modulated through multiplication by $A(f; M, r)$. The sequence is then transformed back to the time domain therefore yielding the realization of $a_g(t)$. The model is therefore fully described by the radiation spectrum, $A(f; M, r)$, and an envelope function, $e_t(t; M, r)$ that will be briefly described in the following.

3.3.1. The radiation spectrum

The radiation spectrum of the model adopted in this work is defined as the product between the source spectrum $E(f; M)$, path effect $P(f; r)$, and site effect $G(f)$:

$$A(f; M, r) = \vartheta E(f; M) P(f; r) G(f) \tag{17}$$

where $\vartheta = (2\pi f)^2$. In Eq. (17) the source spectrum is expressed as:

$$E(f; M) = c M_w S(f; M) \tag{18}$$

where c is a constant that depends on the shear velocity β_s, M_w is the seismic moment which is related to the moment magnitude M through the relationship $\log_{10} M_w = 1.5(M + 10.7)$, while $S(f; M)$ is the displacement source

spectrum. For describing the displacement source spectrum, the two-corner point-source model developed in [18] is used:

$$S(f;M) = \left[\frac{1-e}{1+(f/f_a)^2} + \frac{e}{1+(f/f_b)^2}\right] \tag{19}$$

where the lower corner frequency f_a, higher corner frequency f_b, and weighting parameter e are related to the moment magnitude through the relationships $\log_{10} f_a = 2.181 - 0.496M$, $\log_{10} f_b = 2.41 - 0.408M$, and $\log_{10} e = 0.605 - 0.255M$. For modeling the path effect the following model is adopted [16]:

$$P(f;r) = Z(R_r) \exp\left[\frac{-\pi f R_r}{(Q(f)c_Q)}\right] \tag{20}$$

where $Z(R_r)$ and $Q(f)$ are the geometrical spreading and regional attenuation functions, respectively, while c_Q is the seismic velocity. In the work outlined here, $Q(f)$ is taken as $Q(f) = \alpha_1 f^{\alpha_2}$ with α_1 a geometrical spreading constant and α_2 a geometrical spreading rate. $R_r = \sqrt{h^2 + r^2}$ and represents the radial distance from the earthquake source to the site, with h a moment-dependent equivalent point-source depth that is related to the magnitude through $\log_{10} h = -0.05 + 0.15M$ [18]. In particular, here $Z(R_r) = 1/R_r$ for $R_r < 70$ km and $Z(R_r) = 1/70$ for $R_r > 70$ km [17].

The site effect term of Eq. (17) is taken herein as:

$$G(f) = D(f)A_m(f) \tag{21}$$

where the amplification function $A_m(f)$ can be modeled using empirical curves found in [19] while $D(f)$ is the high-frequency diminution. In particular, the diminution is modeled using the f_{max} filter and therefore as $D(f) = [1 + (f/f_{max})^8]^{-1/2}$ [16].

3.3.2. The time envelope

The role of the envelope function in the point source model is to describe the temporal characteristics of the excitation and is here given by:

$$e_t(t; M, r) = a_t(t/t_n)^{b_t} \exp(-c_t(t/t_n)) \tag{22}$$

where the parameters a_t, b_t, and c_t are calibrated so that the envelope function has a peak value of unity when $t = \lambda_t t_n$ and $e_t(t; M, r) = \eta_t$ when $t = t_n$. In order to achieve this, the parameters are given by $b_t = -\lambda_t \ln(\eta_t)/(1 + \lambda_t(\ln(\lambda_t) - 1))$, $c_t = b_t/\lambda_t$, and $a_t = (\exp(1)/\lambda_t)^{b_t}$ where $t_n = 2T_w$ and is the time duration parameter which depends on the duration of strong ground motion T_w that is given by $1/(2f_a) + 0.05R_r$ [16].

4. The proposed RBDO procedure

Section 2 outlined the type of probabilistic optimization problem that is or interest to this work. In particular, it was observed that the main difficulty in solving the problem is due to the computational effort required to evaluate the reliability constraints, which is compounded by fact that RBDO problems are in general nested problems. That is, while the optimization loop is moving the components of $\mathbf{x}$ within the design space in search of the optimum system, each component move will in general require a probabilistic analysis (or partial probabilistic/sensitivity analysis) to be carried out in order to evaluate the changing reliability constraints. Therefore, as the dimensions of $\mathbf{x}$ increase, so does the overall computational burden.

Here an approach to circumvent this difficulty will be developed based on approximately decoupling the probabilistic analysis from the optimiza-

tion loop through the definition of an optimization sub-problem that can be formulated in a way that is insensitive to the dimensions of $\mathbf{x}$.

4.1. Reformulated problem setting

In order to derive the proposed method, it is first necessary to rewrite the optimization problem in terms of inverse reliability constraints:

$$\text{Find} \qquad \mathbf{x} = \{x_1, ..., x_m\}^T \tag{23}$$

$$\text{to minimize} \qquad W = f(\mathbf{x}) \tag{24}$$

$$\text{s. t.} \quad \tilde{d}_j(\mathbf{x}) - 1 \leq 0 \quad j = 1, ..., N_c \tag{25}$$

$$x_i \in \mathbf{X}_i \quad i = 1, ..., m \tag{26}$$

where $\tilde{d}_j$ is the threshold value of d associated with the target failure probability P_{0_j}. Due to the strictly monotonic nature of the distribution functions associated with the damage measures d_j, the satisfaction of the inverse constraints of Eq. (25) implies the satisfaction of the original constraints of Eq. (3). As in the case of the original RBDO problem, the estimation of the inverse constraints, and so of the thresholds $\tilde{d}_j$, for a given design requires a full probabilistic analysis (simulation) to be carried out during the optimization loop. However, as will be seen in the following, commencing from these constraints it is possible to define an approximate sub-problem with the sought-after properties.

4.2. The Auxiliary Variable Vector (AVV)

In order to derive the sub-problem, it is of interest to consider the following variable that can be defined for each realization of $\mathbf{U}$ (indicated here as

$\mathbf{u}$):

$$\boldsymbol{\Upsilon}_j(\mathbf{u}, \mathbf{x}_0) = \frac{\eta_{R_j}(\mathbf{u}, \mathbf{x}_0)\mathbf{C}_{\mathbf{F}}^{(t)}(\mathbf{u}, \mathbf{x}_0)\boldsymbol{\Gamma}_{R_j}(\mathbf{x}_0)}{\sigma_{R_j}^{(t)}(\mathbf{u}, \mathbf{x}_0)} \tag{27}$$

where $\sigma_{R_j}^{(t)}$ is the standard deviation of the response process $R_j(t)$ in the time statistic sense (i.e. the standard deviation of R_j estimated from the response time history associated with the realization $\mathbf{u}$ of the uncertain vector $\mathbf{U}$), η_{R_j} is the number of standard deviations (in the sense of $\sigma_{R_j}^{(t)}$) that the largest absolute value of $R_j(t)$ is from zero for the event defined by $\mathbf{u}$, while $\mathbf{C}_{\mathbf{F}}^{(t)}$ is the covariance matrix (again to be considered in the sense of the time statistics) of the realization of the following vector-valued stochastic process:

$$\mathbf{F}(t; \mathbf{u}, \mathbf{x}_0) = s_1\mathbf{K}(\mathbf{x}_0)\boldsymbol{\Phi}_n\mathbf{q}_n(t; \mathbf{u}, \mathbf{x}_0) \tag{28}$$

It should be observed that the variables $\sigma_{R_j}^{(t)}$ and $\mathbf{C}_{\mathbf{F}}^{(t)}$ are defined with the intent of giving the largest absolute value of the response process $\hat{R}_j$ a representation that is related to the entire dynamic response process $R_j(t)$ and not just to the instant, $\hat{t}$, at which the peak occurs. Indeed, $\boldsymbol{\Upsilon}_j$ could have been defined simply as $\mathbf{F}$ evaluated in $\hat{t}$. However, a similar approach is often adopted in deterministic dynamic response optimization and is known to cause convergence instabilities [20].

The interest in defining the variable $\boldsymbol{\Upsilon}_j$, whether as $\mathbf{F}(\hat{t})$ or as defined in Eq. (27), derives from the fact that the following relationship holds:

$$\hat{R}_j(\mathbf{u}, \mathbf{x}_0) = \boldsymbol{\Gamma}_{R_j}^T(\mathbf{x}_0)\boldsymbol{\Upsilon}_j(\mathbf{u}, \mathbf{x}_0) \tag{29}$$

The significance of Eq. (29) is that it represents an exact static relationship between $\hat{R}_j$ and the nominal system. In other words, the static application

of $\boldsymbol{\Upsilon}_j$ to the nominal system will generate a response in R_j equal to $\hat{R}_j$. If the right-hand side of Eq. (29) is now divided by the value of the capacity contained in $\mathbf{u}$, the following exact and static relationship is defined between the nominal system and value taken on by the jth damage ratio:

$$d_j(\mathbf{u}, \mathbf{x}_0) = \frac{1}{c_j} \boldsymbol{\Gamma}_{R_j}^T(\mathbf{x}_0) \boldsymbol{\Upsilon}_j(\mathbf{u}, \mathbf{x}_0) \tag{30}$$

So far all quantities have been defined for the event described by $\mathbf{u}$. What is of interest now is to define a similar relationship to that of Eq. (30) for the damage thresholds with target failure probability $\tilde{d}_j$, that is a probabilistic description of the damage ratios occurring over all events. With this in mind, it is necessary to first consider the random capacity written as $C_j = \bar{C}_j(1+\delta_{C_j} C_{n_j})$ where $\bar{C}_j$ is the mean/nominal value of C_j, δ_{C_j} is the coefficient of variation of C_j and C_{n_j} is the normalized (zero mean and unit standard deviation) representation of C_j. At this point it is possible to define the following vector for each realization of $\boldsymbol{\Upsilon}_j$:

$$\boldsymbol{\Upsilon}_{d_j}(\mathbf{u}, \mathbf{x}_0) = \frac{\boldsymbol{\Upsilon}_j(\mathbf{u}, \mathbf{x}_0)}{(1 + \delta_{C_j} c_{n_j})} \tag{31}$$

where c_{n_j} is the normalized component corresponding to the capacity entry c_j of the vector $\mathbf{u}$. As already mentioned, in order to evaluate the reliability constraints (whether in their original or inverse form) for the design point $\mathbf{x}_0$, it is necessary to carry out a simulation in $\mathbf{x}_0$ during which it is possible to define the following Auxiliary Variable Vector (AVV) directly from the samples of $\boldsymbol{\Upsilon}_{d_j}$:

$$\begin{aligned} \tilde{\boldsymbol{\Upsilon}}_j(P_{0_j}, \mathbf{x}_0) &= \bar{\boldsymbol{\Upsilon}}_{d_j}(\mathbf{x}_0) \\ &+ \frac{\eta_{d_j}(P_{0_j}, \mathbf{x}_0) \mathbf{C}_{\boldsymbol{\Upsilon}_{d_j}}(\mathbf{x}_0) \boldsymbol{\Gamma}_{R_j}(\mathbf{x}_0)}{\sigma_{d_j}(\mathbf{x}_0) \bar{C}_j} \end{aligned} \tag{32}$$

where $\bar{\boldsymbol{\Upsilon}}_{d_j}$ is the mean vector of $\boldsymbol{\Upsilon}_{d_j}$ and $\mathbf{C}_{\boldsymbol{\Upsilon}_{d_j}}$ is the covariance matrix of $\boldsymbol{\Upsilon}_{d_j}$, μ_{d_j} and σ_{d_j} are the mean and standard deviation of the damage ratio d_j, while η_{d_j} is the reduced variate indicating the number of standard deviations the threshold value $\tilde{d}_j$ exceeds the mean value of the damage ratio d_j and can be calculated simply as:

$$\eta_{d_j}(P_{0_j}, \mathbf{x}_0) = \frac{\tilde{d}_j(\mathbf{x}_0) - \mu_{d_j}(\mathbf{x}_0)}{\sigma_{d_j}(\mathbf{x}_0)} \tag{33}$$

Because the AVV does not require any significant additional calculations, outside those performed to estimate $\tilde{d}_j$, it can be seen as a by-product of the simulation process and therefore as an auxiliary output of the simulation.

The significance of the AVV, and so of $\tilde{\boldsymbol{\Upsilon}}_j$, is that if it is statically applied to the nominal system, it will generate a response in R that, if divided by the mean/nominal capacity, gives exactly $\tilde{d}_j$:

$$\tilde{d}_j(\mathbf{x}_0) = \frac{1}{\bar{C}_j} \boldsymbol{\Gamma}_{R_j}^T(\mathbf{x}_0) \tilde{\boldsymbol{\Upsilon}}_j(\mathbf{x}_0) \tag{34}$$

The expression of Eq. (34) is particularly useful as it allows the constraints of Eq. (25) to be expressed in a format that is equivalent to a deterministic system loaded by a static distribution in the form of $\tilde{\boldsymbol{\Upsilon}}_j(\mathbf{x}_0)$. As will be explored in the next section, this opens the door to the possibility of defining a particularly useful form of sub-problem.

4.3. The approximate sub-problem

Because of how the AVV was defined, it depends on $\mathbf{x}_0$ and therefore on where in the design space it was calculated. However, this dependency can be assumed relatively weak for moderate changes in the design vector $\mathbf{x}$ around $\mathbf{x}_0$. Indeed $\tilde{\boldsymbol{\Upsilon}}_j$ depends largely on $\boldsymbol{\Upsilon}_j$ (defined in Eq. (31)), which

in turn depends significantly on $\mathbf{F}$ (defined in Eq. 28). By observing that $\mathbf{F}$ can be written as:

$$\begin{aligned}\mathbf{F}(t;\mathbf{u},\mathbf{x}_0) = s_1\mathbf{M}(\mathbf{x}_0)\boldsymbol{\imath}a_g(t;\mathbf{u}) \\ + s_1\mathbf{K}(\mathbf{x}_0)\boldsymbol{\Phi}_n\mathbf{q}_{r_n}(t;\mathbf{u},\mathbf{x}_0)\end{aligned} \tag{35}$$

where $\mathbf{q}_{r_n}$ is the vector of resonant modal responses with components given by:

$$q_{r_j}(t) = q_j(t) - \frac{Q_j(t)}{m_j\left(s_{2_j}\omega_j\right)^2} \tag{36}$$

it is evident that $\mathbf{F}$ has a resonant and background quasi-static component (first term of the right hand side of Eq. (35)). If it is now observed that the majority of mass in a typical building is carried, then the term $\mathbf{M}(\mathbf{x}_0)$ will be relatively insensitive to changes in $\mathbf{x}$. Therefore the background component of $\mathbf{F}$ can be considered independent of $\mathbf{x}_0$ which ultimately results in a weakening of the dependency of $\tilde{\boldsymbol{\Upsilon}}_j$ for small changes in $\mathbf{x}$ around $\mathbf{x}_0$.

This observation allows for the definition of the following optimization sub-problem:

$$\text{Find} \qquad \mathbf{x} = \{x_1, ..., x_m\}^T \tag{37}$$

$$\text{to minimize} \qquad W = f(\mathbf{x}) \tag{38}$$

$$\text{s. t.} \quad \frac{1}{\bar{C}_j}\boldsymbol{\Gamma}_{R_j}^T(\mathbf{x})\tilde{\boldsymbol{\Upsilon}}_j - 1 \leq 0 \quad j = 1, ..., N_c \tag{39}$$

$$x_i \in \mathbf{X}_i \quad i = 1, ..., m \tag{40}$$

where the dependency of $\tilde{\boldsymbol{\Upsilon}}_j$ on $\mathbf{x}$ has been neglected. This assumption effectively decouples the optimization loop from the probabilistic analysis the results of which are now completely contained in the AVV. Indeed, the above outlined optimization sub-problem can be solved without invoking any

probabilistic analysis. The approximation in writing the sub-problem is in how any changes in the design variable vector during the optimization loop are not reflected in $\tilde{\boldsymbol{\Upsilon}}_j$. Therefore, after a solution is found to the sub-problem, it must be reformulated and solved in order to ensure a final design that is absent of any approximations. The fundamental characteristic of the sub-problem that makes it particularly suitable for solving problems with large design variable vectors is in how it is formulated without the need to explore in any way at all the space around $\mathbf{x}_0$. In other words, no sensitivities or function approximations based on partial/local exploration of the design space around $\mathbf{x}_0$ are necessary. Each reformulation simply requires a single probabilistic analysis to be carried out in the current optimal point. This process is commonly denominated as a design cycle and will continue until two successive sub-problems have identical solutions. The total number of design cycles is therefore an indication of the overall efficiency of the proposed procedure as it indicates the number of probabilistic analyses necessary for global convergence.

The classic form of the optimization sub-problem expressed by Eqs (37)-(40) is particularly useful as it allows any well-established optimization methodology to be used for its resolution. In particular, in this work the pseudo-discrete optimality criteria [21, 22] is used therefore allowing the discrete nature of the design space to be fully considered.

5. Case study

5.1. Description

5.1.1. Structural model

In order to investigate the performance of the proposed optimization strategy, a 45-story braced rectangular building with an offset core is considered as a case study (Fig. 1a). The vertical column elements of the structural system are defined by steel box sections grouped in plan as shown in Fig. 1b (C1 to C18). These elements are required to to have a mid-line diameter, D_i, that belong to the discrete set $\{0.2 \text{ m}, 0.25 \text{ m}, 0.3 \text{ m}, 0.35 \text{ m}, ..., 4 \text{ m}\}$ with flange thickness fixed as $D_i/20$. These column elements are grouped over three consecutive floors. The horizontal beam elements of the structural system, indicated as B1 to B6, are located in plan as shown Fig. 1b and are to be designed so as to belong to the standard AISC W24 steel member family [23]. As in the case of the columns, the beams are grouped three floors at a time. The bracing elements are to be designed using the same steel box sections as the columns. In particular, the bracing elements in the X direction are grouped as three separate mega X-braces working over the height of the building. Corresponding braces on the two faces parallel to the X axis of the building are also grouped together. For the Y direction bracing, the elements are once again grouped as three separate mega X-braces working over the height of the building. For this direction the elements of the braced frames are not grouped due to a lack in symmetry the overall system on this direction. The aforementioned grouping of the elements results in a total of 369 independent design groups. The initial structural system is designed with all column elements having a mid-line diameter of 0.6 m while all beam

elements are W24×176 profiles. For the diagonal elements a mid-line diameter of 1.6 m was considered. The floors have an area density of 0.38 t/m^2 and can be assumed rigid in their plane when compared to the flexibility of the horizontal (beam) and vertical (column) elements. Therefore, for modeling the dynamic behavior of the system, three degrees of freedom (two translations in the X and Y directions and one rotation around a vertical axis) are considered for each floor leading to a total of 135 degrees of freedom. The stiffness matrix $\mathbf{K}$ is therefore obtained from static condensation, performed at the centers of mass of each floor, of the full finite element model of the system. The dynamic response of the system is estimated using the procedure presented in Section 3 while considering the first 12 vibration modes, for a total participating mass of over 95% in both the X and Y directions. The initial mean/nominal circular frequencies of the modes are reported in Table 1.

The mean/nominal damping ratios were taken as 1.5% for the first three modes, 2.0% for the next three, 3.0% for the successive three and 4.0% for the final three. The increase in the nominal damping as the mode number increases follows the indications suggested in [24] for steel framed structures. The first six modal frequencies and damping ratios are taken as uncertain while the remaining six take on their nominal values. The uncertain parameters, S_1, S_{2_j} and S_{3_j} with $j = 1, ..., 6$ were modeled as independent lognormal random variables with coefficients of variation 0.025, 0.015, and 0.3 respectively [25], where this last highlights the significant uncertainty that is generally present in the damping of structures.

Table 1: First 12 natural frequencies of the initial structural system

Mode #	Initial frequencies [rad/s]	Final frequencies [rad/s]
1	2.25	3.65
2	4.00	4.24
3	7.20	6.56
4	8.50	10.73
5	13.22	11.92
6	15.89	18.19
7	17.67	18.25
8	19.83	19.88
9	20.68	20.51
10	21.62	23.68
11	24.25	25.30
12	25.71	28.87

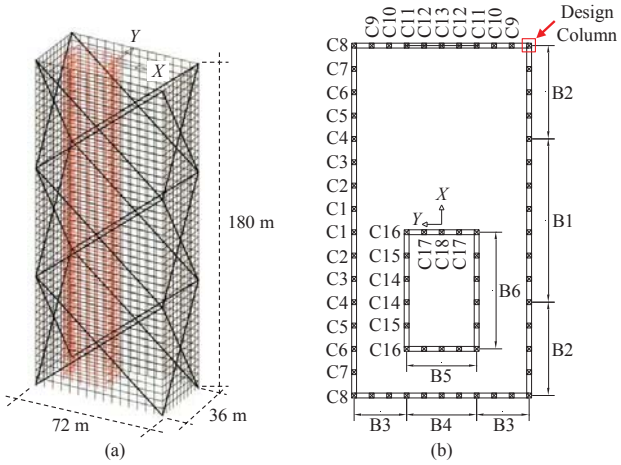

Figure 1: (a) 3D illustration of the case study 45-story building; (b) structural layout of the horizontal and vertical elements as well as the critical column line for the non-structural damage.

5.1.2. Excitation

The stochastic excitation is given by the point source model of Section 3.3. In calibrating the model, a strike slip fault type was considered with model parameters: $\beta_s = c_Q = 750$ m/s; $f_{max} = 30$ rad/s; $\alpha_1 = 300$; $\alpha_2 = 0.3$; $\lambda_t = 0.2$ with $\eta_t = 0.05$ as suggested in [16]. The fault plane distance, r, was taken as a log-normal random variable with a mean distance of 20 km and coefficient of variation 0.4. The moment magnitude, M, was taken as a truncated exponential distribution with $M_{min} = 6$ and $M_{max} = 8$ [26]:

$$p(M) = \frac{\beta \exp[-\beta(M - M_{min})]}{1 - \exp[-\beta(M_{max} - M_{min})]} \tag{41}$$

where the regional seismicity factor is selected as $\beta = 0.7 \ln[10]$. The duration of the simulated stochastic ground accelerations was $T = 100$ s with $\Delta t = 0.01$ s. The total number of components, N_T, of the white noise sequences,

Z, was 10001.

5.1.3. Performance objectives

The objective is to minimize the material weight of the system while ensuring two damage scenarios for ground motions acting down the X and Y directions. The first damage scenario concerns non-structural damage produced by excessive interstory drift occurring over the column line indicated in Fig. 1b in the X and Y directions. The nominal(mean) capacity corresponding to this damage scenario is taken as 1/200 of the inter-story height and is assumed to have a coefficient of variation 0.3 and to be distributed as a log-normal random variable. The second damage scenario is associated with excessive combined axial and flexural stress occurring in the critical fiber of each of the 369 design groups. In this case, the response process is given by:

$$R(t;\mathbf{u}) = f_N(t;\mathbf{u}) + f_{M_x}(t;\mathbf{u}) + f_{M_\mathcal{Y}}(t;\mathbf{u}) \tag{42}$$

where $f_N(t;\mathbf{u})$ is the axial stress response process while $f_{M_x}(t;\mathbf{u})$ and $f_{M_\mathcal{Y}}(t;\mathbf{u})$ are the flexural stress response processes due to moments acting around the local $\mathcal{X}$ and $\mathcal{Y}$ axes of the member. The associated structural capacity is taken to have a nominal (mean) value of 3.4×10^5 kN/m^2 and to be distributed as a log-normal random variable with coefficient of variation 0.1. In assessing the maximum stresses, a deterministic live load of 2 kN/m^2 is also considered distributed over each floor.

It is worth noting that a linear load-effect model is considered adequate for describing the response of the seismically excited systems considered here as this work is primarily focused on modeling the response of high-rise structures which tend to have large design variable vectors but relatively moderate

response to earthquakes, or at least a response that is desirable to keep linear.

5.1.4. Optimization algorithm

The design variable vector $\mathbf{x}$ is taken as the mid-line diameters, D_i, of the box sections while, for the standard W24 sections, the cross sectional area is considered. These section properties can be related to the other mechanical properties of the section (moments of inertia, shear areas, etc.) following the relationships presented in [27, 15] for the box sections, while for the standard W24 sections the relationships outlined in [21] can be used. This implies that each of the 369 design groups will be assigned a single design variable leading to a total dimension for $\mathbf{x}$ of 369.

In order to solve the optimization sub-problems, the procedure outlined in [28] is adopted. Therefore the stress-based constraints are reduced to movable lower limits on the design variable vector, while the drift-based constraints are reduced to explicit functions of $\mathbf{x}$ through the use of the principle of virtual work. Because the objective function is also explicit in $\mathbf{x}$, the sub-problem can be efficiently solved using a pseudo-discrete optimality criteria algorithm [22, 21]. In formulating the sub-problem at each design cycle, the thresholds with target failure probabilities, $\tilde{d}_j$, are estimated by assuming the failure probabilities, P_{f_j}, follow a log-normal distribution which is calibrated by simulating 4000 samples of $\mathbf{U} = \{C_j, S_1, \mathbf{S}_{2_n}^T, \mathbf{S}_{3_n}^T, r, \mathbf{Z}^T\}^T$, with $n = 6$. Recalling the dimension of $\mathbf{Z}$, this leads to a total dimension for $\mathbf{U}$ is 10016 while the total number of constraints is 918 ($N_c = 918$), 45 drift-based constraints evaluated in the X and Y directions for ground motions acting down the X or Y direction as well as 369 stress-based constraints also

evaluated for ground motions acting down the X or Y direction. Considering the size of the design variable vector, $m = 365$, the case study truly represents a large scale RBDO optimization problem.

5.2. Results

As mentioned in Section 5.1.4, in evaluating the failure probabilities associated with the constraints, a log-normal distribution is assumed. This choice was made on the basis of the high number of basic random variables following log-normal distributions for this type of problem.To verify this assumption a Monte Carlo simulation was carried out on the initial system using 20000 samples and compared to calibrated log-normal failure distributions. Figure 2 shows this comparison for the Y direction top floor drift-based damage ratio and the stress-based damage ratio of the column group C8 between floors 1 and 3. As can be seen, the log-normal assumption would seem reasonable even if some tendency to over-estimate the failure probabilities for high threshold levels would seem evident. This result is seen for all other damage ratios. Although the log-normal assumption was made here, it should be observed that the procedure presented in this work does not require the failure probabilities to follow a log-normal distribution. It was assumed here for computational convenience.

Figure 2 shows the initial and final failure probabilities associated with the occurrence of non-structural damage due to excessive drift over the column line indicated in Fig. 1. In particular, Fig. 3 shows the X and Y direction response. As can be seen, the initial system does not meet the constraints placed on the occurrence of non-structural damage for ground motions acting in the X or Y direction. With respect to the structural dam-

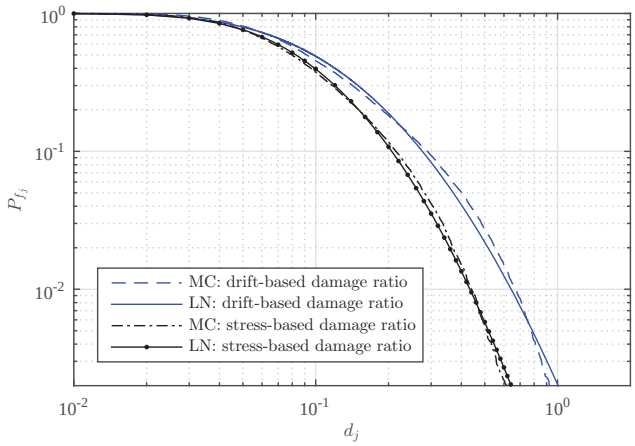

Figure 2: Comparison between the calibrated log-normal (LN) failure distribution and the Monte Carlo (MC) estimated failure distributions. The drift-based damage ratio is the top floor Y direction response for Y direction ground motion while the stress-based damage ratio is for the column group C8 between floors 1 and 3 with X direction ground motion.

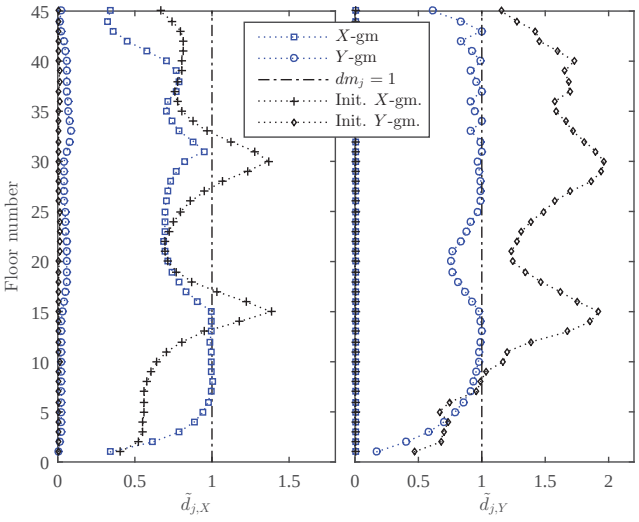

Figure 3: Initial and optimized non-structural damage measure thresholds with target failure probability $P_{0_j} = 10^{-3}$ for the design column line indicated in Fig. 1.

age constraints, Fig. 4 shows that the initial system once again does not meet all performance constraints. In applying the proposed optimization strategy,

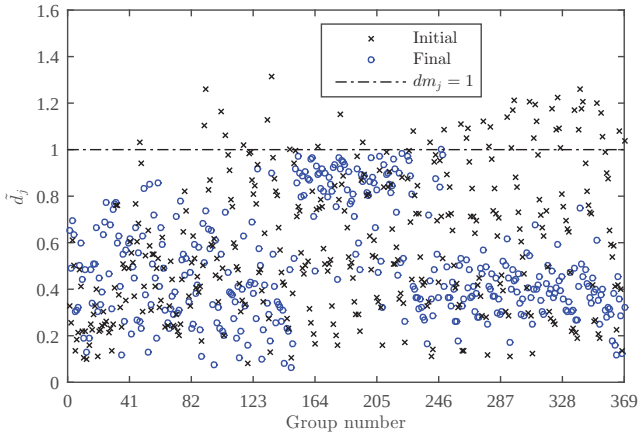

Figure 4: Initial and optimized structural damage ratio thresholds with target failure probability $P_{0_j} = 10^{-3}$. The maximum thresholds for X and Y ground motions are shown.

it can be seen from Figs. 3 and 4 that the optimized system meets all imposed performance constraints. In particular, looking at Fig. 3 it can be seen that the system has a number of active, or near active, constraints for ground motions acting in both the X and Y directions. This clearly attests to the strong convergence properties of the proposed approach. The strong and steady convergence properties of the proposed approach are clearly illustrated by the design history of the objective function of Fig. 5. In particular, for all intents and purposes, the problem convergences after only 15 design cycles and therefore probabilistic analyses. This result is quite remarkable as it represents a very small fraction of the analyses that would be necessary to directly solve a problem of this size and complexity. From Fig. 6

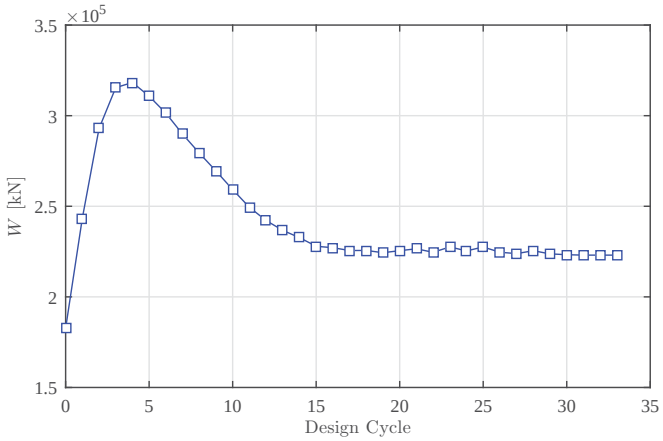

Figure 5: Objective function design cycle history.

it can also be seen that the structure practically meets all performance requirements by design cycle 15 with the remaining design cycles serving as a fine tuning of the problem. In particular, for the case study considered here the convergence criteria was strictly set as obtaining two successive designs defined by identical design variable vectors. The fact that the algorithm met such a strict criteria once again attests to the convergence properties of the proposed approach. Figure 5 shows that the final optimized structural system is only around 23% heaver than the original system notwithstanding the significant performance enhancement achieved. It is interesting to note from Table 1 that, even though the system has become stiffer in the Y direction in order to satisfy the drift-based constraints that were significantly violated by the initial system, overall the initial and optimum systems have relatively similar natural frequencies, with some actually increasing for the optimum system, indicating how the optimization algorithm is effectively searching

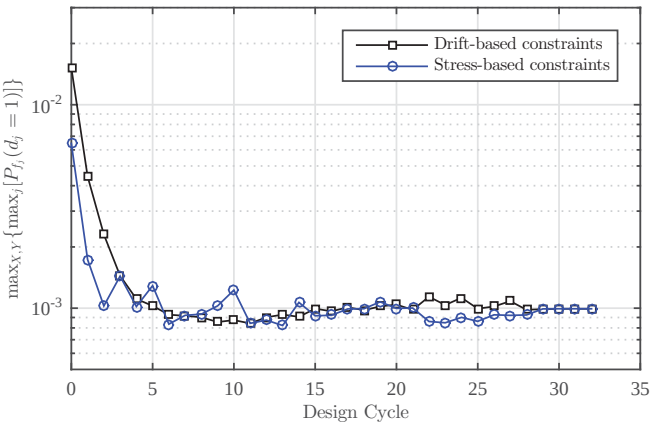

Figure 6: Convergence history of the maximum (for ground motions coming from the X or Y direction) component failure probabilities for the structural and non-structural damage scenarios.

for the most flexible (and therefore least seismically susceptible) system that satisfies the performance constraints. Finally it should be remembered that the sub-problems were solved using a discrete optimization algorithm, made possible without complication due to the simple and classic from assumed by the sub-problems, therefore resulting in a discrete final design variable vector that belongs to the sets $\mathbf{X}_i$ for $i = 1, ..., m$. This is illustrated in Table 2 where the initial and final discrete mid-line diameters of the corner column group C8 are reported showing how the final column sizes belong to the set defined in Sec. 5.1.1. Table 2 also gives an indication of how the optimal system works. Indeed, the corner columns are towards the upper limit of the associated feasible set and practically vary only between successive X-bracings, which indicates that the optimal structure is a 3D braced mega-system.

Table 2: Initial and final section sizes for design group C8.

Floor number	Initial size [cm]	Final size [cm]
1-3	60	345
4-6	60	355
7-9	60	360
10-12	60	355
13-15	60	355
16-18	60	280
19-21	60	275
22-24	60	280
25-27	60	285
28-30	60	275
31-33	60	100
34-36	60	90
37-39	60	70
40-42	60	55
43-45	60	55

6. Conclusions

This paper presented an efficient framework for the design optimization of large-scale uncertain systems driven by non-stationary stochastic excitation. In particular, the proposed method was specifically developed to solve practical reliability-based design optimization problems posed on uncertain dynamic systems that are defined by large-scale design variable vectors as well as reliability constraints written in terms of high-dimensional probabilistic integrals. The proposed approach is based on approximately decoupling the inherently nested probabilistic analysis loop from the optimization loop through the definition of an optimization sub-problem that can be formulated from information gathered from a single simulation-based probabilistic analysis carried out in the current design point. In particular, the sub-problem is formulated through the definition of a probabilistic auxiliary variable vector (AVV) that may be estimated as a simple by-product of the simulation process without the need to invoke any significant additional calculations. Because the sub-problem takes on a simple deterministic form, it can be efficiently solved by any well-established optimization algorithm. By formulating and solving a sequence of sub-problems, a series of steadily improving designs are defined, leading to a solution to the original problem at a fraction of the computational cost necessary to directly solve the original optimization problem. The practicality and strong convergence properties of the proposed approach were illustrated on a full scale high-rise building example subject to non-stationary stochastic earthquake excitation.

Acknowledgements

This research effort is supported by the University of Michigan. This support is gratefully acknowledged.

References

[1] Jensen, H.A., Valdebenito, M.A., Schuëller, G.I.. An efficient reliability-based optimization scheme for uncertain linear systems subject to general gaussian excitation. Comput Methods Appl Mech Engrg 2008;198(1):72–87.

[2] Valdebenito, M.A., Schuëller, G.I.. A survey on approaches for reliability-based optimization. Struct Multidisc Optim 2010;42:645–663.

[3] Taflanidis, A.A.. Reliability-based optimal design of linear dynamical systems under stochastic stationary excitation and model uncertainty. Eng Struct 2010;32:1446–1458.

[4] Jensen, H.A., Kusanovic, D.S., Valdebenito, M.A., Schuëller, G.I.. Reliability-based design optimization of uncertain stochastic systems: gradient-based scheme. J Eng Mech 2012;138:60–70.

[5] Royset, J.O., Der Kiureghian, A., Polak, E.. Reliability-based optimal structural design by the decoupling approach. Reliab Eng Syst Safe 2001;73(3):213–221.

[6] Du, X., Chen, W.. Sequential optimization and reliability assessment method for efficient probabilistic design. ASME J Mech Des 2004;126(2):225–233.

[7] Zou, T., Mahadevan, S.. A direct decoupling approach for efficient reliability-based design optimization. Struct Multidisc Optim 2006;31:190–200.

[8] Valdebenito, M.A., Schuëller, G.I.. Efficient strategies for reliability-based optimization involving non-linear, dynamical structures. Comput Struct 2011;89:1797–1811.

[9] Schuëller, G., Pradlwarter, H., Koutsourelakis, P.. A critical appraisal of reliability estimation procedures for high dimensions. Probab Eng Mech 2004;19:463–474.

[10] Yang, T.Y., Moehle, J., Stojadinovic, B., Der Kiureghian, A.. Seismic performance evaluation of facilities: methodology and implementation. J Struct Eng 2009;135(10):1146–1154.

[11] Federal Emergency Management Agency (FEMA), . Seismic performance assessment of buildings, Volume 1 Methodology (FEMA Publication P-58-1). Washington, DC; 2012.

[12] Spence, S.M.J., Kareem, A.. Tall buildings and damping: a concept-based data-driven model. J Struct Eng 2014;140(5):04014005–1–15.

[13] Spence, S.M.J., Bernardini, E., Guo, Y., Kareem, A., Gioffrè, M.. Natural frequency coalescing and amplitude dependent damping in the wind-excited response of tall buildings. Prob Eng Mech 2014;35:108–117.

[14] Li, Y.S., Kareem, A.. Recursive modeling of dynamic-systems. J Eng Mech 1990;116:660–679.

[15] Spence, S.M.J., Kareem, A.. Data-enabled design and optimization (DEDOpt): Tall steel buildings frameworks. Comput Struct 2013;134(12):134–147.

[16] Boore, D.M.. Simulation of ground motion using the stochastic method. Pure Appl Geophys 2003;160:635–676.

[17] Vetter, C., Taflanidis, A.A.. Global sensitivity analysis for stochastic ground motion modeling in seismic-risk assessment. Soil Dyn Earthq Eng 2012;38:128–143.

[18] Atkinson, G.M., Silva, W.. Stochastic modeling of California ground motions. Bull Seismol Soc Am 2000;90:255–274.

[19] Boore, D.M., Joyner, W.B.. Site amplifications for generic rock sites. Bull Seismol Soc Am 1997;87:327–341.

[20] Kang, B.S., Park, G.J., Arora, J.S.. A review of optimization of structures subjected to transient loads. Struct Multidisc Optim 2006;31:81–95.

[21] Chan, C.M., Grierson, D.E., Sherbourne, A.N.. Automatic optimal design of tall steel building frameworks. J Struct Eng 1995;121(5):838–847.

[22] Spence, S.M.J.. Time domain non-gaussian optimization of wind excited tall buildings under vulnerability constraints. Ph.D. thesis; University of Florence and TU Braunschweig; 2009.

[23] AISC, . Specification for Structural Steel Buildings. American Institute of Steel Construction (AISC), Chicago, IL; 2010.

[24] Satake, N., Sude, K., Arakawa, T., Sasaki, A., Tamura, Y.. Damping evaluation using full-scale data of buildings in Japan. J Struct Eng 2003;129(4):470–477.

[25] Bernardini, E., Spence, S.M.J., Kwon, D.K., Kareem, A.. Performance-based design of high-rise buildings for occupant comfort. J Struct Eng http://dx.doi.org/10.1061/(ASCE)ST.1943-541X.0001223;.

[26] Kramer, S.L.. Geotechnical Earthquake Engineering. Upper Saddle River, New Jersey: Prentice-Hall, Inc.; 1996.

[27] Spence, S.M.J., Gioffrè, M.. Efficient algorithms for the reliability optimization of tall buildings. J Wind Eng Ind Aerodyn 2011;99(6-7):691–699.

[28] Spence, S.M.J., Kareem, A.. Performance-based design and optimization of uncertain wind-excited dynamic building systems. Eng Struct 2014;:In Press.